SpaceOps-2025, ID #503

Experimental Verification of Attitude Estimation with Magnetometer Bias Estimation in Spinning CubeSats Using Kalman Filter: Validation with VICON System

Sajad S Afshari, Xue Nemoga-Stout, Julia Ryznar, Giannis Georgiou, Spencer Ryznar, Philip Ferguson

Department of Mechanical Engineering, University of Manitoba, Canada
sajadsa@umanitoba.ca

Abstract

This paper presents an experimentally validated Extended Kalman Filter (EKF) framework for real-time attitude determination and magnetometer bias estimation in spinning CubeSats. The proposed approach augments the conventional quaternion-based EKF by directly modeling both gyroscope and magnetometer biases as part of the system state, enabling in-situ calibration without relying on time-consuming ground-based or pre-launch procedures. A three-axis gimbal system equipped with a CubeSat Attitude Determination and Control System (ADCS) board was used to simulate various spin rates (5–15 RPM), while a VICON motion capture system provided precise ground-truth attitude reference. Experimental results demonstrate that incorporating magnetometer and gyroscope biases in the EKF state reduces estimation errors compared to baseline methods that neglect bias dynamics. The filter converges to stable bias estimates within an acceptable time. This performance advantage is particularly beneficial for small satellites operating under stringent power and computational constraints, where frequent sensor calibrations are impractical. Overall, the findings underscore the viability of this EKF approach for CubeSat-class missions, confirming that online bias estimation can reliably refine magnetometer-based attitude solutions under realistic spinning conditions. The method's effectiveness in a laboratory test bed, combined with its minimal computational footprint, makes it applicable to resource-constrained space platforms. Future work will extend the filter to incorporate other sensor modalities and investigate adaptive tuning strategies for varying on-orbit environments, aiming to further improve reliability and autonomy of CubeSat attitude determination and control systems.

Keywords: CubeSat; Magnetometer Bias; Quaternion EKF; Spinning Spacecraft; VICON Motion Capture; Attitude Determination

1 Introduction

Small satellites, particularly CubeSats, have spurred significant interest in the aerospace community due to their low cost, reduced mass, and rapid development cycle. As these platforms grow in popularity, the demand for reliable yet power-efficient and cost-effective attitude determination systems intensifies [1, 2]. One of the most attractive sensor options in this context is the magnetometer, primarily due to its capability to measure Earth's magnetic field vector with acceptable accuracy, its low power consumption, and its small footprint. These advantages are crucial for CubeSats, which often operate under severe resource constraints.

Unfortunately, magnetometer-based attitude estimation can be compromised by biases induced by onboard magnetic disturbances (such as residual magnetic dipoles from electronics) and sensor hardware imperfections [3]. If not properly calibrated, these biases can lead to significant degradation in attitude solutions, especially during demanding operational phases like detumbling or spinning maneuvers. Traditional calibration methods typically employ offline procedures that are performed either on the ground or at the beginning of the mission [4]; while effective for initial alignment, such methods do not account for time-varying bias drifts and changes in the spacecraft's internal magnetic environment. Consequently, there is a growing need for in-situ, autonomous calibration methods that can adapt to evolving spacecraft conditions in real time.

There has been studies in the literature that have highlighted the simultaneous estimation of spacecraft attitude and sensor biases via Kalman filtering, showcasing that such approaches can be implemented under CubeSat-class computational budgets [5, 6]. Notably, early work in EKF-based attitude estimators revealed the filter's ability to incorporate noise and measurement uncertainties, providing a framework for spacecraft Attitude Determination and Control System (ADCS) [7]. More recent efforts have emphasized the importance of reliable, self-contained calibration algorithms that can operate under spinning or detumbling phases and that can incorporate both gyroscope and magnetometer biases [3, 5]. This is particularly relevant when gyroscope calibrations are also needed on-orbit, thereby minimizing the risk of accumulating measurement errors that degrade the entire attitude determination solution.

Attitude motion determination using a minimal set of sensors is an equally attractive approach to further reduce the mass, volume, and power budgets in small satellites [8]. In extreme miniaturization scenarios, such as picosatellites, even small savings in sensor size or power consumption become critical. Although star sensors typically provide the most accurate measurements [9], their higher cost and power demands can be prohibitive for certain small satellite missions. Likewise, sun sensors alone cannot offer full observability of the three-axis attitude motion, and their measurements are unavailable during eclipse [10]. Angular velocity sensors, while useful, require additional vector observations to disambiguate attitude states and estimate drifting biases [11].

Some studies have proposed Kalman filter variants to tackle the real-time estimation of both attitude and magnetometer bias using only onboard data [12,13]. These approaches often rely on the time evolution of the Earth's magnetic field along the satellite's orbit, enabling attitude motion tracking through magnetometer vector measurements. However, a persistent challenge lies in the fact that many small satellites install magnetometers inside the spacecraft bus rather than on deployable booms [14]. This leads to large and varying offsets stemming from electromagnetic interference caused by internal circuitry, solar panels, antennas, and battery charging processes. Accordingly, researchers have proposed a methods such as extended Kalman filters (EKF) for simultaneously estimating these biases and the spacecraft's attitude quaternion [4, 15].

A relevant study in also focuses on practical calibration techniques, including magnetometer bias compensation at the system level. Surveys on existing magnetometer calibration procedures detail both offline and in-flight bias estimation approaches, often highlighting the necessity of these techniques for accurate and reliable performance [13]. For instance, real-time bias estimation algorithms that do not depend on prior knowledge of attitude have been proposed [16], and further refinements have been introduced using sliding windows or averaging approaches [17]. In some cases, the algorithms account for additional calibration parameters such as scale factors, axis misalignments, and even time-varying biases [18]. Despite the theoretical maturity of these real-time calibration methods, literature on their empirical validation, and an investigation of the errors and performance under different body rates, remains relatively scarce.

In an effort to address these gaps, this paper presents an experimentally validated Extended Kalman Filter (EKF) framework for real-time attitude determination and sensor bias estimation in spinning CubeSats. The filter models both gyroscope and magnetometer biases as part of the state vector. Building on the principles of Kalman filtering for spacecraft attitude estimation [7, 19], we designed a systematic experimental setup

that subjects the Attitude Determination and Control System (ADCS) board of a 6U CubeSat engineering model to spin rates of 30–90 degrees per second using a three-axis gimbal.

Ground truth orientation data are provided by a VICON motion capture system. To ensure precise reference measurements using VICON cameras, we also performed validation tests to assess the accuracy of VICON for spacecraft attitude angle measurements. By comparing the results from the proposed EKF with those from a baseline filter that neglects bias estimation, as well as with the ground truth from the VICON system, we demonstrate that including bias terms substantially reduces the root mean square error (RMSE) of the attitude estimation. We also investigate the relationship between estimation error and angular velocity to identify the spin rates at which the estimation error is minimized. Our results show that the filter converges to stable estimates within an acceptable time, offering a promising pathway for CubeSat-class missions that require reliable, autonomous attitude determination, especially when high-end sensors are not used due to cost constraints.

The remainder of this paper is structured as follows. Section 2 details the EKF formulation, including the process and measurement models. Our experimental setup is described in Section 3, with a focus on practical considerations for using VICON cameras to provide reliable ground truth for attitude determination problems. In Section 4, we present our findings, highlighting the improvements in attitude estimation achieved by accounting for sensor biases, along with a discussion of the filter's performance in comparison with the VICON system. Finally, Section 5 concludes the paper by summarizing the major contributions and outlining directions for future research aimed at enhancing the reliability and autonomy of CubeSat attitude determination and control systems.

2 Methodology

Here, we present a real-time attitude determination framework using an Extended Kalman Filter (EKF) that includes sensor biases as part of the filter's state vector. The filter estimates the satellite's attitude quaternion $\mathbf{q}(t)$, gyroscope bias $\delta\mathbf{b}_g(t)$, and magnetometer bias $\delta\mathbf{b}_m(t)$, offering in-orbit calibration capabilities for low-cost sensors in CubeSats.

Unlike conventional offline calibration techniques, which are sensitive to long-term sensor drift caused by aging, thermal gradients, or electromagnetic interference, the presented approach maintains performance during extended safe-mode or detumbling operations. The EKF combines real-time body-frame sensor measurements with inertial magnetic field data obtained from the International Geomagnetic Reference Field (IGRF) model, as detailed in the following sections.

2.1 Process Model and Prediction Step

The EKF state vector is defined as:

$$\mathbf{x} = \begin{bmatrix} q_0 & q_1 & q_2 & q_3 & b_{g_x} & b_{g_y} & b_{g_z} & b_{m_x} & b_{m_y} & b_{m_z} \end{bmatrix}^T, \tag{1}$$

where $\mathbf{q} = [q_0, q_1, q_2, q_3]^T$ represents the quaternion defining the transformation from the inertial frame to the body frame. The parameters $\mathbf{b}_g$ and $\mathbf{b}_m$ denote the gyroscope and magnetometer biases in different directions, respectively. To avoid the singularities and rank-deficiency issues discussed in Lefferts et al. [7], the EKF update step omits q_0 as a free parameter. Instead, q_0 is reconstructed using the unit-norm constraint:

$$q_0 = \sqrt{1 - q_1^2 - q_2^2 - q_3^2}, \tag{2}$$

and the quaternion is renormalized after each correction step to preserve $\|\mathbf{q}\| = 1$. The quaternion evolves based on the gyroscopic angular velocity:

$$\dot{\mathbf{q}} = \frac{1}{2}\mathbf{\Omega}(\boldsymbol{\omega})\mathbf{q}, \tag{3}$$

where

$$\boldsymbol{\omega} = \mathbf{u} - \delta\mathbf{b}_g - \boldsymbol{\eta}_g, \tag{4}$$

with $\mathbf{u}$ representing the raw gyroscope reading and $\boldsymbol{\eta}_g$ the additive Gaussian noise. The gyroscope and magnetometer biases are modeled as random walks:

$$\dot{\delta\mathbf{b}}_g = \boldsymbol{\eta}_{bg}, \quad \dot{\delta\mathbf{b}}_m = \boldsymbol{\eta}_{bm}. \tag{5}$$

The discrete-time EKF prediction step is expressed as:

$$\mathbf{x}_k^- = f(\mathbf{x}_{k-1}^+), \tag{6}$$
$$\mathbf{P}_k^- = \mathbf{F}_k \mathbf{P}_{k-1}^+ \mathbf{F}_k^T + \mathbf{Q}_k, \tag{7}$$

where $\mathbf{F}_k = \left.\frac{\partial f}{\partial \mathbf{x}}\right|_{\mathbf{x}_{k-1}^+}$ is the Jacobian of the system dynamics and $\mathbf{Q}_k$ is the process noise covariance matrix.

2.2 Measurement Model and Update Step

The magnetometer provides measurements of the Earth's magnetic field in the body frame. The measurement model is:

$$\mathbf{B}_{\text{meas},k} = \mathbf{A}(\mathbf{q}_k)\mathbf{B}_{\text{IGRF},k} + \delta\mathbf{b}_m + \boldsymbol{\nu}_k, \tag{8}$$

where:

- $\mathbf{A}(\mathbf{q}_k)$ is the direction cosine matrix derived from the quaternion $\mathbf{q}_k$,
- $\mathbf{B}_{\text{IGRF},k}$ is the magnetic field vector in the inertial frame obtained from the IGRF model [20] at the spacecraft's location and time,
- $\boldsymbol{\nu}_k$ is zero-mean Gaussian measurement noise.

The IGRF model is queried using onboard ephemeris data (position and time), and returns $\mathbf{B}_{\text{IGRF},k}$ in the Earth-Centered Inertial (ECI) frame.

The measurement function is:

$$\mathbf{h}(\mathbf{x}_k) = \mathbf{A}(\mathbf{q}_k)\mathbf{B}_{\text{IGRF},k} + \delta\mathbf{b}_m. \tag{9}$$

The Jacobian matrix $\mathbf{H}_k$ used in the EKF correction step is:

$$\mathbf{H}_k = \begin{bmatrix} \frac{\partial(\mathbf{A}(\mathbf{q}_k)\mathbf{B}_{\text{IGRF},k})}{\partial \mathbf{q}_k} & \mathbf{0}_{3\times 3} & \mathbf{I}_{3\times 3} \end{bmatrix}, \tag{10}$$

where $\frac{\partial \mathbf{A}(\mathbf{q})\mathbf{B}}{\partial \mathbf{q}}$ is the quaternion-to-vector rotation Jacobian, computed analytically or using established approximations from quaternion calculus.

The EKF update equations are then:

$$\mathbf{K}_k = \mathbf{P}_k^- \mathbf{H}_k^T \left(\mathbf{H}_k \mathbf{P}_k^- \mathbf{H}_k^T + \mathbf{R}_k\right)^{-1}, \tag{11}$$
$$\mathbf{x}_k^+ = \mathbf{x}_k^- + \mathbf{K}_k \left[\mathbf{B}_{\text{meas},k} - \mathbf{h}(\mathbf{x}_k^-)\right], \tag{12}$$
$$\mathbf{P}_k^+ = (\mathbf{I} - \mathbf{K}_k \mathbf{H}_k)\mathbf{P}_k^-, \tag{13}$$

followed by renormalization of the quaternion to maintain the unit-norm constraint:

$$\mathbf{q}_k^+ \leftarrow \frac{\mathbf{q}_k^+}{\|\mathbf{q}_k^+\|}. \tag{14}$$

2.3 Observability Analysis

The observability of our system is governed by the spacecraft's rotational motion and available measurements. In our case, the filter state includes the attitude quaternion $\mathbf{q} \in \mathbb{R}^4$, gyroscope bias $\delta\mathbf{b}_g \in \mathbb{R}^3$, and magnetometer bias $\delta\mathbf{b}_m \in \mathbb{R}^3$, yielding a total of 10 states. For nonlinear systems such as ours, local observability can be assessed through the rank of the observability matrix, constructed using successive Lie derivatives of the output function with respect to the system dynamics [21]. In the EKF context, a

practical and widely accepted criterion is to evaluate the local rank condition of the linearized observability matrix [22]:

$$\mathcal{O} = \begin{bmatrix} \mathbf{H}_k \\ \mathbf{H}_k\mathbf{F}_k \\ \mathbf{H}_k\mathbf{F}_k^2 \\ \vdots \\ \mathbf{H}_k\mathbf{F}_k^{n-1} \end{bmatrix} \in \mathbb{R}^{n\times 10}, \tag{15}$$

where $\mathbf{F}_k = \frac{\partial f}{\partial \mathbf{x}}$ is the system Jacobian, and $\mathbf{H}_k = \frac{\partial h}{\partial \mathbf{x}}$ is the measurement Jacobian linearized about the current state. Full local observability requires that $\text{rank}(\mathcal{O}) = 10$.

In the specific case of magnetometer-only updates, the observability of gyroscope and magnetometer biases is strongly influenced by the richness of the spacecraft's motion. Static or low-excitation motion results in a rank-deficient observability matrix, making some bias components unobservable or weakly observable. However, when the satellite undergoes sufficient rotational excitation—such as spinning or tumbling—magnetometer measurements in the body frame span multiple directions over time, providing the necessary excitation to render the full state observable. This is further supported by the structure of the measurement Jacobian $\mathbf{H}_k$, which includes:

$$\mathbf{H}_k = \left[\frac{\partial(\mathbf{A}(\mathbf{q}_k)\mathbf{B}_{\text{IGRF},k})}{\partial \mathbf{q}_k},\ \mathbf{0}_{3\times 3},\ \mathbf{I}_{3\times 3} \right]. \tag{16}$$

The sensitivity of the measurement to quaternion components depends on the alignment between the rotated magnetic field vector and the principal axes. Therefore, without rotation (especially about all three axes), the derivative with respect to certain quaternion components becomes nearly linearly dependent, diminishing the observability of associated biases.

Simulations and analytical studies (e.g., [4]) have confirmed that the inclusion of persistent rotational dynamics—especially with non-zero angular rates about all axes—ensures sufficient excitation for full-state observability. In our configuration, the CubeSat's inherent spin during detumbling and safe-mode operations naturally satisfies this condition. Therefore, under the assumption of continuous spacecraft rotation with a non-zero component along each principal axis, the proposed system becomes locally observable. Considering the explained methodology, Algorithm 1 summarizes the step-by-step framework used in this paper. In the next section, we present the experimental setup for validating the proposed framework.

3 Experimental Setup and VICON Motion Capture

To validate our attitude estimation algorithm, we developed a testbed that integrates the ADCS board of a 6U CubeSat engineering model with a VICON motion capture system. The CubeSat ADCS board features the BNO055 multi-sensor module, which provides real-time measurements of angular velocity and magnetic field strength. Mounted on a 3-axis gimbal, the board is capable of simulating 3-DOF angular motion to emulate the rotational dynamics of a satellite in orbit (Fig. 1). The ADCS system samples sensor data at a rate of 50 Hz. The VICON system, comprising an array of infrared cameras operating at 100 Hz, tracks reflective markers attached to the test article. Before conducting our attitude estimation verification tests, we conduct experiments on the VICON system to ensure its accuracy and reliability to be used as a ground truth for our validation tests.

3.1 Validating VICON Motion Capture System

Our VICON system used for spacecraft attitude determination is shown in Figure 2. The VICON motion capture system provides sub-millimeter positional and high rotational accuracy [23], making it an excellent ground truth reference for our experiments. Our setup comprised 12 infrared cameras: 6 VICON Vero v2.2 cameras, and 6 Vicon Valkyrie VK26 cameras, all capturing data at 100 Hz. The cameras were arranged to maximize coverage and minimize blind spots within the capture volume. Calibration was performed using a VICON calibration wand with known marker geometry, establishing the camera orientation and

Algorithm 1 EKF for Attitude and Bias Estimation

Input: Initial state $\mathbf{x}_0$, covariance $\mathbf{P}_0$, noise covariances $\mathbf{Q}_k, \mathbf{R}_k$
Measurements: Gyroscope $\mathbf{u}_k$, magnetometer $\mathbf{B}_{\text{meas},k}$, IGRF field $\mathbf{B}_{\text{IGRF},k}$
Initialize: $\mathbf{x}_0 = [\mathbf{q}_0, \delta\mathbf{b}_{g,0}, \delta\mathbf{b}_{m,0}]^T$, $\mathbf{P}_0$
for each timestep $k = 1, 2, \ldots$ **do**
▷ Prediction Step
  $\boldsymbol{\omega}_k \leftarrow \mathbf{u}_k - \delta\mathbf{b}_{g,k-1}$
  $\mathbf{q}_k^- \leftarrow \mathbf{q}_{k-1}^+ + \frac{1}{2}\boldsymbol{\Omega}(\boldsymbol{\omega}_k)\mathbf{q}_{k-1}^+ \cdot \Delta t$
  $\delta\mathbf{b}_{g,k}^- \leftarrow \delta\mathbf{b}_{g,k-1}^+$
  $\delta\mathbf{b}_{m,k}^- \leftarrow \delta\mathbf{b}_{m,k-1}^+$
  $\mathbf{x}_k^- \leftarrow [\mathbf{q}_k^-, \delta\mathbf{b}_{g,k}^-, \delta\mathbf{b}_{m,k}^-]^T$
  Compute $\mathbf{F}_k = \frac{\partial f}{\partial \mathbf{x}}$
  $\mathbf{P}_k^- \leftarrow \mathbf{F}_k\mathbf{P}_{k-1}^+\mathbf{F}_k^T + \mathbf{Q}_k$
▷ update Step
  $\hat{\mathbf{B}}_k \leftarrow \mathbf{A}(\mathbf{q}_k^-)\mathbf{B}_{\text{IGRF},k} + \delta\mathbf{b}_{m,k}^-$
  $\mathbf{r}_k \leftarrow \mathbf{B}_{\text{meas},k} - \hat{\mathbf{B}}_k$
  Compute $\mathbf{H}_k = \frac{\partial h}{\partial \mathbf{x}}$
  $\mathbf{K}_k \leftarrow \mathbf{P}_k^-\mathbf{H}_k^T(\mathbf{H}_k\mathbf{P}_k^-\mathbf{H}_k^T + \mathbf{R}_k)^{-1}$
  $\mathbf{x}_k^+ \leftarrow \mathbf{x}_k^- + \mathbf{K}_k\mathbf{r}_k$
  $\mathbf{P}_k^+ \leftarrow (\mathbf{I} - \mathbf{K}_k\mathbf{H}_k)\mathbf{P}_k^-$
  Recompute $q_0 = \sqrt{1 - q_1^2 - q_2^2 - q_3^2}$; normalize $\mathbf{q}_k^+$
end for

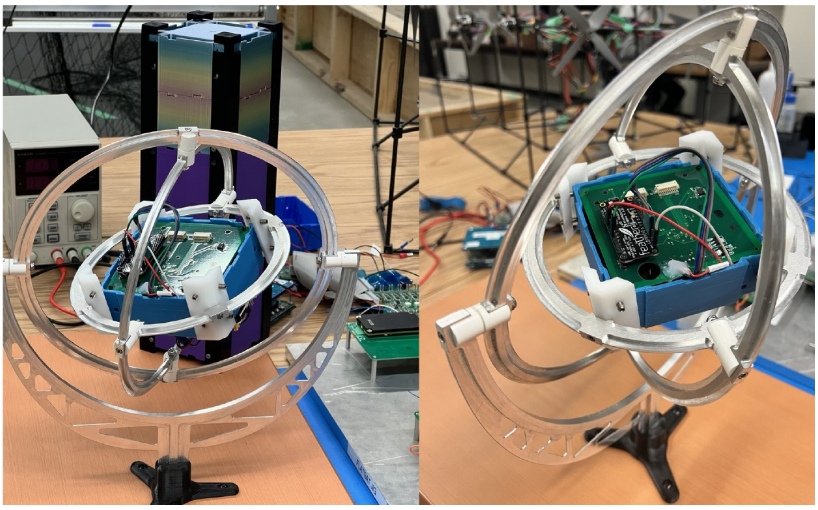

Figure 1: Close-up of the 3-axis gimbal setup with the CubeSat engineering model. The ADCS board, containing the BNO055 multi-sensor module, is mounted at the center.

the global x-, y-, and z-axes. The VICON Tracker 3.10 software generated real-time 3D pose data for the CubeSat, including both position and orientation (attitude) using tracked marker sets. To verify the system's accuracy in capturing rotational dynamics, we conducted a controlled experiment using a motor rotating at a known rate of 15 RPM (i.e., 90°/s). We recorded 8404 frames during which the motor completed exactly 21 rotations, resulting in an average of 400.2 frames per rotation. At 100 Hz sampling, this corresponds to 4.002 s per rotation, yielding a measured rate of 14.99 RPM (89.94°/s). The rotational rate error is therefore just 0.06°/s (0.07%), which confirms the VICON system's high precision in tracking angular motion. Additionally, since the VICON system reconstructs full 6-DOF pose data, it provides direct access to the time-varying orientation of the tracked body.

Figure 2: Overview of the VICON motion capture laboratory. The netted capture area is surrounded by 12 cameras arranged to track reflective markers at 100 Hz.

3.2 Coordinate Frame Alignment and Offset Calculation

A close-up of the gimbal arrangement is presented in Figure 1. During initial testing, a small but consistent misalignment was observed between the CubeSat's sensor-frame axes and the coordinate system defined by the VICON motion capture system. To ensure meaningful comparisons between sensor-based attitude estimates and VICON-derived ground truth, we transformed both datasets into a common reference frame. To this end, we took the following steps:

Step 1: Extract Initial Sensor Orientation. At system initialization, with the CubeSat placed in a known rest orientation (aligned with the global frame), we recorded the initial Euler angles reported by the onboard sensor. These angles were computed under static conditions using the sensor's internal fusion algorithm, which combines data from the accelerometer and magnetometer. The measured initial orientation error was:

$$\boldsymbol{e}_{\text{sensor}} = \begin{bmatrix} 0.0873^\circ \\ -0.0182^\circ \\ -0.6862^\circ \end{bmatrix}, \tag{17}$$

corresponding to roll (ϕ), pitch (θ), and yaw (ψ) in the ZYX convention.

Step 2: Define the Target Frame. We define our reference frame — the "identity" frame — as one having zero rotation about all three axes:

$$\boldsymbol{e}_{\text{identity}} = \begin{bmatrix} 0^\circ \\ 0^\circ \\ 0^\circ \end{bmatrix}. \tag{18}$$

Step 3: Convert Euler Angles to Rotation Matrices. Using standard ZYX Euler-to-matrix conversion functions, we computed the rotation matrices corresponding to the initial sensor orientation and the identity frame:

$$R_{\text{sensor}} = R_z(\psi)R_y(\theta)R_x(\phi), \tag{19}$$

$$R_{\text{identity}} = I_{3\times 3}. \tag{20}$$

Substituting the values from Equation (17) and converting to radians, we obtained:

$$R_{\text{sensor}} \approx \begin{bmatrix} 0.9999 & 0.0120 & -0.0003 \\ -0.0120 & 0.9998 & 0.0015 \\ 0.0005 & -0.0014 & 0.9999 \end{bmatrix}.$$

Step 4: Compute Offset Matrix. We solved for the rotation offset matrix R_{offset} such that:

$$R_{\text{offset}}R_{\text{sensor}} = R_{\text{identity}}. \tag{21}$$

This yields:

$$R_{\text{offset}} = R_{\text{sensor}}^{-1}. \tag{22}$$

Using numerical inversion:

$$R_{\text{offset}} \approx \begin{bmatrix} 0.9999 & -0.0120 & 0.0003 \\ 0.0120 & 0.9998 & -0.0015 \\ -0.0005 & 0.0014 & 0.9999 \end{bmatrix}.$$

Step 5: Apply Offset to All Sensor Readings. For each time step t, we converted the raw Euler angles $\boldsymbol{e}_{\text{sensor}}(t)$ into a rotation matrix $R_{\text{sensor}}(t)$, then applied the precomputed offset:

$$R_{\text{corrected}}(t) = R_{\text{offset}}R_{\text{sensor}}(t). \tag{23}$$

This process aligns all sensor data to the same reference frame used for VICON measurements. The corrected sensor dataset, now expressed in the same frame, allows for direct comparison with ground truth, supporting our validation of the attitude estimation algorithm.

3.3 Data Synchronization and Alignment

Accurate synchronization between the CubeSat sensor data and VICON measurements was essential to ensure valid comparisons of the observed angular trajectories. While the sensor data were recorded at 50 Hz and the VICON data at 100 Hz, a straightforward resampling of the VICON data alone does not guarantee phase alignment. Even a 10–20 ms slip in synchronization can produce noticeable discrepancies in the measured spin profiles and lead to erroneous conclusions about system performance. To address this challenge, we employed a hybrid synchronization approach combining both manual and mathematical calibration technique as follows.

The first step involved matching the known start and stop times of the experimental runs. We recorded both sets of data (sensor and VICON) concurrently with a shared clock reference. The VICON data were then downsampled to 50 Hz to match the sensor sampling rate. This alignment ensured that both datasets began and ended at roughly the same absolute timescale. To refine the synchronization, we identified repeatable features in the angular velocity and orientation data. Specifically, we located easily distinguishable "peaks" in the rotation signals. By comparing the time indices of these matching peaks, we measured any residual offset remaining after the initial time alignment. After applying the above adjustments, we visually inspected the overlaid sensor and VICON signals. In cases where the automatic feature matching suggested ambiguous or multiple candidate offsets, a small manual time shift was introduced. This step reduced discrepancies around critical points in the spin profiles, ensuring that the two datasets overlapped. For completeness, a cross-correlation algorithm was also tested on the data to objectively compute the time delay that maximizes signal similarity.

4 Results and Discussion

Table 1 summarizes the configuration of the EKF parameters and experimental settings. The gyroscope and magnetometer were each sampled at 50 Hz, while the VICON motion capture system provided ground-truth pose data at 100 Hz. Attitude spin rates varied between 30°/sec and 90°/sec (i.e., 5–15 RPM), enabling validation of the filter performance across low and moderate angular velocities.

Further insight is provided by Figure 4, which plots mean attitude estimation error against body angular velocity. The plot shows higher body rates tend to increase estimation errors, reflecting the EKF's greater sensitivity to unmodeled sensor dynamics at faster rotation speeds. Nonetheless, the filter converges and tracks with higher accuracy in most rates, when biases are explicitly modeled. When biases being modeled, the estimator exhibits reduced error, remaining closer to the ground truth over the duration of the test.

Table 1: Experimental Configuration and Parameters

Parameter	**Value / Description**
Gyro sampling rate	50 Hz
Magnetometer sampling rate	50 Hz
VICON capture rate	100 Hz
Spin rate range	30 °/sec-90 °/sec
Initial bias uncertainty	$\pm 50\,\mu T$ for magnetometer

Figure 3 illustrates the estimated attitude angles versus time for each axis, compared with the ground truth data provided by the VICON camera set. It can be seen that all estimated attitude angles deviate more noticeably from the VICON ground truth when the bias is not considered in the estimator. This reduction in error when incorporating biases demonstrates that accounting for bias across the magnetometer axes enhances the filter's ability to estimate the satellite's attitude more reliably. For small satellite applications, this method is particularly valuable, as it enables prompt and autonomous in-orbit calibration—crucial when using low-cost sensors. The estimated magnetometer biases over 120 seconds are also illustrated in Figure 5. Clearly, the biases did not converge within this period. However, the improved agreement between the estimated attitude and the VICON reference in Figure 3 indicates that the filter is trending correctly toward bias estimation.

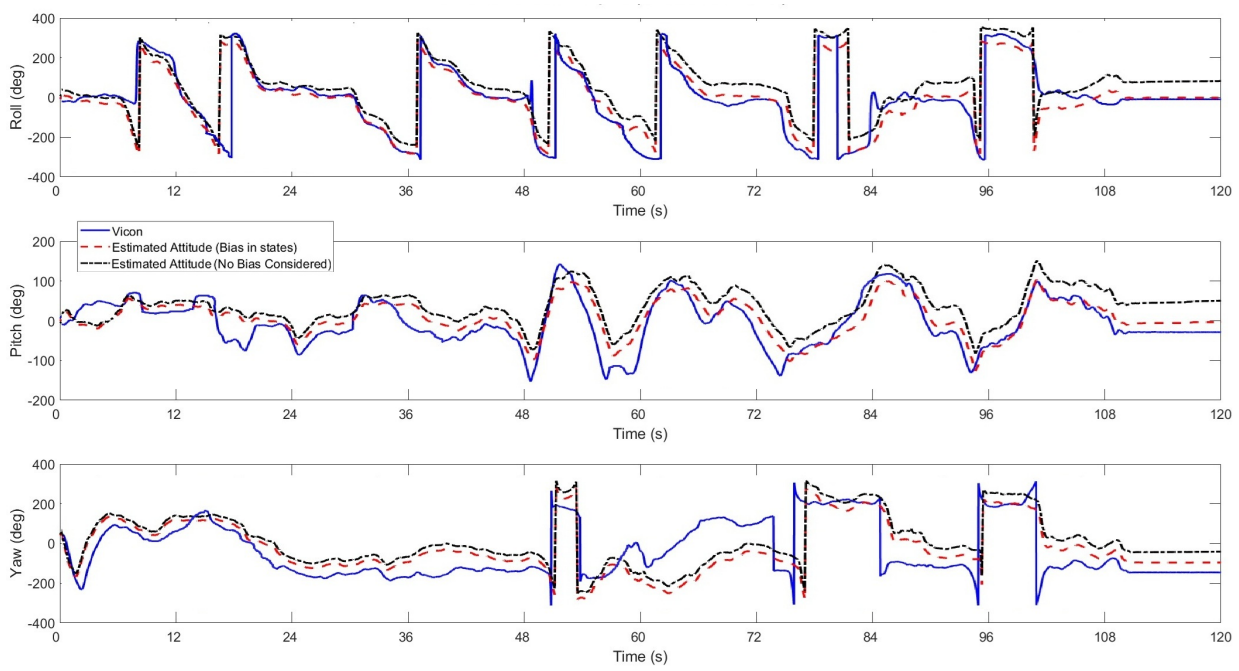

Figure 3: Estimated attitude angles over time, compared to VICON ground truth. Each plot illustrates attitude estimation results from the EKF with and without incorporating bias estimation, demonstrating the improved accuracy achieved when biases are explicitly considered.

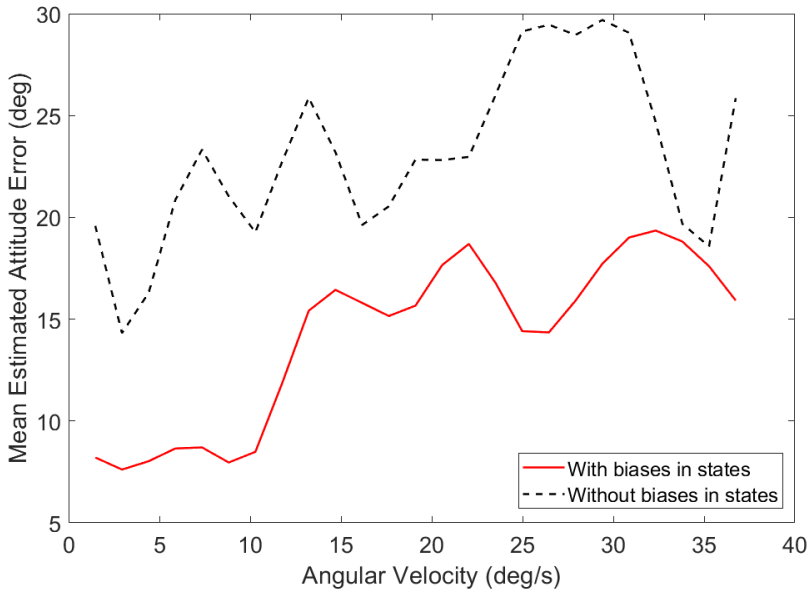

Figure 4: Mean attitude estimation error vs. angular rates.

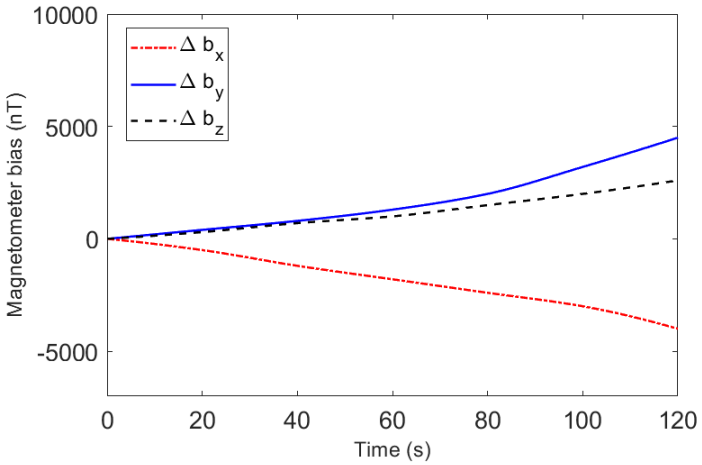

Figure 5: Estimated magnetometer biases in diffrent axis.

Figure 6 presents the root-mean-square (RMS) attitude estimation errors (in degrees) for roll, pitch, and yaw, comparing results from two scenarios, when gyroscope and magnetometer biases are estimated in the EKF state vector, and when no bias estimation is included. The RMS values, calculated from the difference between the estimated and VICON-measured (ground-truth) orientations, show that including bias estimation reduces errors across all three axes.

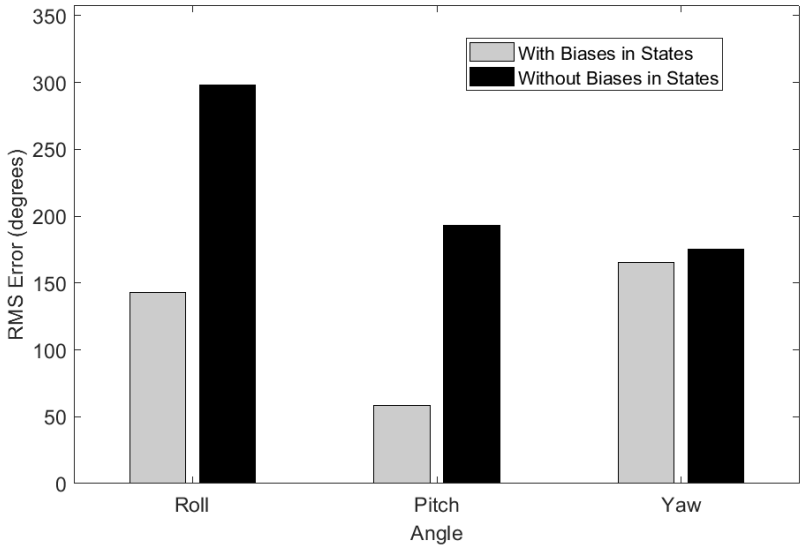

Figure 6: Root-mean-square (RMS) attitude estimation error using EKF with and without including biases in states.

Although accuracy is improved by bias estimation, still a residual discrepancy of about 10 degrees (or less) remains between the EKF estimates and the VICON reference. These deviations likely stem from sensor noise, minor experimental misalignments, and unmodeled nonlinearities. In addition, accuracy is generally better at lower spin rates, consistent with the premise that higher angular velocities might amplify biases and measurement noise.

Despite these errors, the results confirm that the proposed EKF framework can achieve attitude determination under biased sensor conditions, which is critical when using low-cost sensors. By estimating biases on

orbit, the need for pre- or post-launch calibration procedures can be reduced, making this approach particularly attractive for cubeSat missions. For spin-stabilized platforms, nominal rotation inherently enhances bias observability in magnetometer readings, further streamlining in-orbit calibration. As a result, a decent attitude knowledge can be established during early mission stages, such as safe-mode recovery, thereby improving satellite reliability and operational flexibility.

Collectively, these VICON-based experiments indicate the feasibility of implementing the presented EKF architecture in flight. The successful real-time bias estimation not only improves orientation accuracy but also highlights the practical utility of low-cost sensors for efficient and robust CubeSat attitude determination. Moreover, the methodology presented here for validating attitude estimation using the VICON system provides a valuable approach for future design reviews and pre-launch testing of various spacecraft.

5 Conclusion

This paper has presented and experimentally validated an EKF-based framework for real-time attitude determination in small satellites, with estimation of gyroscope and magnetometer biases. A key feature of our methodology is the reliance on low-cost sensors to achieve an accurate attitude estimate. Through a series of controlled ground experiments, we subjected the ADCS board of a 6U CubeSat engineering model to spin and tracked its orientation using a VICON motion capture system. This testing procedure allowed us to verify the filter's accuracy and validate our EKF solution for attitude estimation when sensor biases are considered in the estimation process. The results demonstrate that ignoring sensor biases can lead to degradation in attitude accuracy, especially under higher spin rates. In contrast, the proposed EKF framework incorporating bias states achieved lower RMS errors across all axes, underscoring the importance of in-situ, autonomous bias calibration. Moreover, the VICON validation campaigns confirmed that attitude errors remain within acceptable bounds for many small-satellite missions, particularly those operating with low-cost sensors. These findings are particularly relevant to the next generation of low-cost small satellite missions, where budget limitations often force trade-offs between sensor precision and mission requirements. By autonomously taking into account biases in attitude estimation, our approach reduces the need for extensive pre-deployment calibration and mitigates issues related to drift or internal electromagnetic interference. As a result, developers can utilize inexpensive sensor packages without incurring a commensurate decrease in overall attitude knowledge—a critical capability for missions that rely on spinning or detumbling phases to achieve initial stabilization. In future work, we plan to extend our framework to incorporate advanced sensor fusion techniques or integrate data from secondary sensors (e.g., coarse sun sensors or horizon sensors) to further bolster robustness. Additionally, on-orbit demonstrations will provide a definitive assessment of the filter's performance under realistic operational conditions, paving the way for more autonomous and reliable CubeSat ADCS architectures.

Acknowledgments

This project is undertaken with the financial support of the Canadian Space Agency.

References

[1] J. R. Wertz, *Spacecraft Attitude Determination and Control*. Dordrecht: D. Reidel, 1978.

[2] Z. Zhang, J. Xiong, and J. Jin, "On-orbit real-time magnetometer bias determination for micro-satellites without attitude information," *Chinese Journal of Aeronautics*, vol. 28, no. 5, pp. 1503–1509, 2015.

[3] S. Ghosh and E. G. Lightsey, "A real-time on-orbit magnetometer calibration method for cubesats," *Acta Astronautica*, vol. 185, pp. 288–299, 2021.

[4] H. E. Söken and S.-i. Sakai, "Real-time attitude-independent magnetometer bias estimation for spinning spacecraft," *Journal of Guidance, Control, and Dynamics*, vol. 41, no. 1, pp. 276–279, 2018.

[5] J. Smith and E. Clarke, "On-orbit magnetometer bias estimation for small satellites: A comparative study," *Journal of Spacecraft and Rockets*, vol. 59, no. 4, pp. 1112–1125, 2022.

[6] D. Li and J. Kalski, "Implementation of real-time extended kalman filter for magnetometer and gyro bias calibration in cubesats," *Aerospace Science and Technology*, vol. 116, p. 106929, 2021.

[7] E. J. Lefferts, F. L. Markley, and M. D. Shuster, "Kalman filtering for spacecraft attitude estimation," *Journal of Guidance, Control, and Dynamics*, vol. 5, no. 5, pp. 417–429, 1982.

[8] M. L. Orozco and B. S. Giraldo, "Attitude determination and control in small satellites: A review," *IEEE Journal on Miniaturization for Air and Space Systems*, 2024.

[9] B. M. Bomani, "Cubesat technology past and present: Current state-of-the-art survey," Tech. Rep., 2021.

[10] J. Mata Garcia, "Implementation and verification of attitude determination control algorithms for a 3u cubesat," 2023.

[11] H. Al-Jlailaty and M. M. Mansour, "Efficient attitude estimators: A tutorial and survey," *Journal of Signal Processing Systems*, vol. 94, no. 11, pp. 1309–1343, 2022.

[12] S. B. Farahan, J. J. Machado, F. G. de Almeida, and J. M. R. Tavares, "9-dof imu-based attitude and heading estimation using an extended kalman filter with bias consideration," *Sensors*, vol. 22, no. 9, p. 3416, 2022.

[13] J. S. Bennett, B. E. Vyhnalek, H. Greenall, E. M. Bridge, F. Gotardo, S. Forstner, G. I. Harris, F. A. Miranda, and W. P. Bowen, "Precision magnetometers for aerospace applications: A review," *Sensors*, vol. 21, no. 16, p. 5568, 2021.

[14] J. R. Kopacz, R. Herschitz, and J. Roney, "Small satellites an overview and assessment," *Acta Astronautica*, vol. 170, pp. 93–105, 2020.

[15] D. Ivanov, D. Roldugin, S. Tkachev, M. Ovchinnikov, R. Zharkikh, A. Kudryavtsev, and M. Bychek, "Attitude motion and sensor bias estimation onboard the siriussat-1 nanosatellite using magnetometer only," *Acta Astronautica*, vol. 188, pp. 295–307, 2021.

[16] A. Fornasier, Y. Ng, C. Brommer, C. Böhm, R. Mahony, and S. Weiss, "Overcoming bias: Equivariant filter design for biased attitude estimation with online calibration," *IEEE Robotics and Automation Letters*, vol. 7, no. 4, pp. 12 118–12 125, 2022.

[17] D. Benli, "Designing computationally light algorithms for concurrent real-time attitude estimation and sensor calibration," Master's thesis, Middle East Technical University (Turkey), 2023.

[18] S. Rodríguez-Martínez and G. Troni, "Full magnetometer and gyroscope bias estimation using angular rates: Theory and experimental evaluation of a factor graph-based approach," *IEEE Journal of Oceanic Engineering*, 2025.

[19] F. L. Markley and J. L. Crassidis, *Fundamentals of Spacecraft Attitude Determination and Control*. Springer, 2014.

[20] C. Kloss and C. Beggan, "The 14th generation of the international geomagnetic reference field," Copernicus Meetings, Tech. Rep., 2025.

[21] T. Berger, T. Reis, and S. Trenn, *Observability of linear differential-algebraic systems: A survey*. Springer, 2017.

[22] A. Katriniok and D. Abel, "Adaptive ekf-based vehicle state estimation with online assessment of local observability," *IEEE Transactions on Control Systems Technology*, vol. 24, no. 4, pp. 1368–1381, 2015.

[23] Vicon Motion Systems, *Vicon Vantage and Vicon Tracker Technical Specifications*, 2020, available online: https://docs.vicon.com/display/VUD.